韓國港灣學會 第11卷 第2號, pp.241~255. 1997.

論 文

Development of Simulation Model for Diffusion of Oil Spill in the Ocean I

- Three Dimensional Characteristics of the Circulation in the Nearly Closed Bay -

J.W. Lee · K.C. Kim** · S.Y. Kang* · D.H. Doh**

해양유출기름의 확산 시뮬레이션 모델 개발 I

- 폐쇄만에서의 3차원 흐름특성분석 -

이중우 · 김기철 · 강신영 · 도덕희

Key Words : three dimensional model(3차원 모델), $k-\varepsilon$ turbulence closure model($k-\varepsilon$난류 클로즈 모델), eddy(소용돌이), warm water discharge(온배수), wind-driven current(풍성류), compensational effect(상호보완작용)

Abstract

Three dimensional numerical model is used to simulate the circulation patterns in the Gamcheon Bay located in Pusan, Korea and compared with the observed data. The model is forced by winds, tidal elevation at open boundaries, and warm water discharged from the outfall of power plant, Turbulence mixing coefficients are calculated according to a $k-\varepsilon$ turbulence closure submodel. Temperature, salinty and current are measuted extensively and these measuted data are compared with the simulation results. Eddy-like features exist both in observed data dna simulation results. These eddies are the results of interaction with the weak tidal current, wind driven current and warm water discharges. Compensational deeects are also found to exist such that while surface current is strong, bottom current tends to weaken and vice versa.

1. Introduction

Analysis of the circulation in the nearly closed bay is complicated because of the interactions of tidal current, winds, buoyant plumes of fresh water or warm water from power plant, coastline

* 정회원, 한국해양대학교 교수
** 정회원, 동아대학교 해양공학과 교수

geometry and bottom topography. Numerical models were used to simulate the circulation characteristics of the nearly closed bay and applied to the Gamcheon bay comparing with the observations. Depth-integrated xy-models or width-averaged xz-models do not properly reproduce the inetraction between the existing current field and the buoyant plume. The vertical variations in density, velocity and in addition complex coastline geometry can seriously change the basic structure of the circulation patterns. The three dimensional models in coastal areas are initiated by Leendertse and Liu(1), Heaps(2), Sundermann(3)and have been continued by other researchers. But application of the model to the real geometry requires deep physical insights and considerable effort to parameter the non-dimensional terms. The most difficult problem is to set the turbulent diffusion coefficients. In this paper, we present some results of three dimensional numerical simulation of circulation in Gamcheon bay. Turbulent diffusion coefficients are calculated using $k-\varepsilon$ turbulence closure submodel.

Gamcheon bay is located at Busan, Korea. It is enclosed by the land except the entrance of 200m width between two breakwaters located southern part of the area(Fig. 1). Flow in the bay is very weak because tidal forcing is limited by narrow entrance. The purpose of this study is (i) to study the mixing processes of warm water discharged from the outfall, the velocity and temperature structures in the bay and to understand how these structures are affected by winds and different tidal ranges;
(ii) to apply the three dimensional model to understand the basic dynamics which control the hydrodynamics of the bay; (iii) to compare the observation data and the results of numerical simulation to test the general applicability of the model.

2. Field observations

Location and bathymetry of Gamcheon bay is shown in Fig. 1. Gamcheon bay has somewhat elongated shape in north-southward. It is bounded with the open sea by the breakwater. It has nearly constant depth of 12m except near the breakwater where the depth reaches to 16m. Because of narrow entrance between two breakwaters, the flow in Gamcheon bay is very weak. Tidal effect seems to be weak while duarable winds affect the flow pattern of Gamcheon bay somewhat strongly.

Temperatures and salinities are measured using CTD(Conductivity-Temperature-Depth) on February 26 (1st.) and May 17, 1996(2nd.) on the stations denoted in Fig. 2. February 26, 1996 corresponds to neap tides and May 17, 1996 to spring tides. At each station, SBE 19 CTD of Sea-Bird Electronics was lowered to 1m above the bottom, taking two samples of temperature, conductivity and pressure per second. Surface temperature distributions for 1st. and 2nd. measurements are shown in Fig. 3, 4. In Fig. 3, isotherms run nearly northwest-southeast, shows higher temperature on east side. The measurements were conducted during flood tides in 1st survey. Measured current data shows that flood current flows stronger on west side so that advection effect would have resulted in the distribution of isotherms as in Fig. 3. Second CTD measurements were conducted during ebb tide. Ebb tidal current flows mainly along the west side coast so that the distributions of isotherms in Fig. 4 show higher temperature on west side except near the outfall where tongue-like patterns toward west exist.

To find out the flow fields, Eulerian measurements for 1 tidal period on the stations denoted in Fig. 2 and Lagrangian tracking of surface flow by the drogue were conducted on February 28(1st.), May 18(2nd.) and July 26(3rd.), 1996 . Two Aanderra current meters are moored at surface and bottom for Eulerian measurements of current. First Lagrangian tracking is represented in Fig. 5. Two drogues were tracked — outside and inside the breakwater. The result shows pecurior and complicated flow patterns. The drogue dropped at 10:25 am. which was two hours after low water so that it would be expected to flow toward inner side of Gamcheon bay. But it flowed toward the breakwater southeastward. This flow pattern suggests the existence of eddy structure which may be the result of two water masses — one is northward flood current and the other is southward flow originated from the mixing of warm water discharge and existing ebb current. Near the breakwater, the flow pattern is very complicated. At inner part of bay, the flow is very weak so that it is expected large wind effect on the flow pattern. Fig. 6 shows 2nd Lagrangian tracking. It shows strong east-west flow outside the breakwater while oscillatory flow pattern exist in the central part of the bay. Third measurement shows similar patterrns to those of 2nd measurement(Fig. 7). Eulerian currents in the bay do not represent the tidal period but oscillates at the period of about 30 minute(Fig. 8a,b) which also suggests the existence of eddy structure.

3. The Model

The basic equations of the model solve for surface elevation, three dimensional velocities, temperature, salinity and density fields using continuity equation for incompressible fluids, three dimensional Navier Stokes equation and conservation of temperature and salt equations. For simplicity, two approximations are applied. One is hydrostatic approximation which neglects advection and vertical acceleration so that the weight of the fluid identically balances the pressure. The other is Boussinesq assumption so that density differences are neglected unless they are multiplied by gravity.

The model uses orthogonal Cartesian coordinates with x increasing eastward, y increasing northward, and z increasing vertically upwards. The free surface is at $z=\eta(x, y, t)$, the bottom at $z=-H(x, y)$, and $z=0$ is mean tidal level. The continuity equation is

$$\frac{\partial u}{\partial x}+\frac{\partial v}{\partial y}+\frac{\partial w}{\partial z}=0 \quad \cdots\cdots (1)$$

and momentum equations are

$$\frac{\partial u}{\partial t}+u\frac{\partial u}{\partial x}+v\frac{\partial u}{\partial y}+w\frac{\partial u}{\partial z}-fv = -\frac{1}{\rho_0}\frac{\partial p}{\partial x}+\frac{\partial}{\partial z}\left(K_M\frac{\partial u}{\partial z}\right)+F_x \quad \cdots\cdots (2)$$

$$\frac{\partial v}{\partial t}+u\frac{\partial v}{\partial x}+v\frac{\partial v}{\partial y}+w\frac{\partial v}{\partial z}+fu = -\frac{1}{\rho_0}\frac{\partial p}{\partial y}+\frac{\partial}{\partial z}\left(K_M\frac{\partial v}{\partial z}\right)+F_y \quad \cdots\cdots (3)$$

$$\rho g=-\frac{\partial p}{\partial z} \quad \cdots\cdots (4)$$

where u, v, w denote ensemble mean velocities in the x, y , and z directions respectively; f is the Coriolis parameter$=2\Omega\sin\phi$ (Ω; angular speed of the Earth, ϕ; latitude); ρ is the mean density and ρ_0 is a reference density; g is the gravitational acceleration and p is the pressure; K_M is the vertical turbulent viscosity; F_x and F_y are horizontal friction terms to be defined shortly.

The conservation equations for temperature and salinity are

$$\frac{\partial T}{\partial t}+u\frac{\partial T}{\partial x}+v\frac{\partial T}{\partial y}+w\frac{\partial T}{\partial z}=\frac{\partial}{\partial z}(K_H\frac{\partial T}{\partial z})+F_T \quad \cdots\cdots(5)$$

$$\frac{\partial S}{\partial t}+u\frac{\partial S}{\partial x}+v\frac{\partial S}{\partial y}+w\frac{\partial S}{\partial z}=\frac{\partial}{\partial z}(K_H\frac{\partial S}{\partial z})+F_S \quad \cdots\cdots(6)$$

where T is mean temperature; S is mean salinity; K_H is vertical turbulent diffusivity; F_T and F_S are horizontal diffusion terms of temperature and salinity respectively.

Density is calculated by the following equation.(4)

$$\frac{\partial S}{\partial t}+u\frac{\partial S}{\partial x}+v\frac{\partial S}{\partial y}+w\frac{\partial S}{\partial z}=\frac{\partial}{\partial z}(K_H\frac{\partial S}{\partial z})+F_S \quad \cdots\cdots(7)$$

$$\begin{aligned}\rho &= \rho_0+\Delta\rho \\ &= (5890+38T-0.375T^2+3S)/[(1779.5 \\ &+11.25T-0.0745T^2)-(3.8+0.01T)S \\ &+0.698(5890+38T-0.375T^2+3S)]\end{aligned} \quad \cdots\cdots(8)$$

The terms F_X, F_y, F_T and F_S represent horizontal mixing processes. The horizontal mixing processes have wide ranges of length scale so that all of the motions induced by small-scale processes are not resolved by the model grid and cannot be adequately represented by mathematical form. In analogy to molecular diffusion, these can be written as

$$F_x=\frac{\partial}{\partial x}[2K_M\frac{\partial u}{\partial x}]+\frac{\partial}{\partial y}[K_M(\frac{\partial u}{\partial y}+\frac{\partial v}{\partial x})] \quad \cdots\cdots(9)$$

$$F_y=\frac{\partial}{\partial y}[2K_M\frac{\partial v}{\partial y}]+\frac{\partial}{\partial x}[K_M(\frac{\partial u}{\partial y}+\frac{\partial v}{\partial x})] \quad \cdots\cdots(10)$$

$$F_{T,S}=\frac{\partial}{\partial x}[2K_H\frac{\partial(T,S)}{\partial x}]+\frac{\partial}{\partial y}[K_H\frac{\partial(T,S)}{\partial y}] \quad \cdots(11)$$

To close the basic equations listed above, vertical turbulent viscosity K_M and vertical turbulent diffusivity K_H should be parameterized adequately. In this study, $k-\varepsilon$ turbulent model given by McGuirk and Rodi(5) is applied. The equation for turbulent kinetic energy is

$$\frac{\partial k}{\partial t}+u\frac{\partial k}{\partial x}+v\frac{\partial k}{\partial y}+w\frac{\partial k}{\partial z}=\frac{\partial}{\partial z}(\frac{K_M}{\sigma_k}\frac{\partial k}{\partial z})+P_v+G_w-\varepsilon+F_k \quad \cdots\cdots(12)$$

$$\frac{\partial \varepsilon}{\partial t}+u\frac{\partial \varepsilon}{\partial x}+v\frac{\partial \varepsilon}{\partial y}+w\frac{\partial \varepsilon}{\partial z}=\frac{\partial}{\partial z}(\frac{K_M}{\sigma_\varepsilon}\frac{\partial \varepsilon}{\partial z})+\frac{\varepsilon}{k}(C_{1\varepsilon}P_v-C_{2\varepsilon}\varepsilon) \quad \cdots\cdots(13)$$

where k is the turbulent kinetic energy; $P_v=K_M[(\frac{\partial u}{\partial z})^2+(\frac{\partial v}{\partial z})^2]$, turbulence production term; F_k, horizontal diffusion term, is similar to eq. (10); $G_w=\frac{g}{\rho_0}K_H\frac{\partial \rho}{\partial z}$, buoyancy term; ε is turbulent dissipation rate. $C_{1\varepsilon}$ and $C_{2\varepsilon}$ is constant related by(6)

$$C_{1\varepsilon}=C_{2\varepsilon}-\frac{\chi^2}{\sigma_\varepsilon C_\mu^{0.5}} \quad \cdots\cdots(14)$$

where the value of $C_{2\varepsilon}$ is known between 1.8 and 2.0; χ is von Karman constant; C_μ is $(\overline{u'w'}/k)^2$ at local equilibrium shear layer and is known as 0.09 (u', v' are turbulent fluctuation velocities). $C_{1\varepsilon}$ is changed according to the value of χ. Various values are tested in the analysis so that appropriate value of 1.6 is chosen.

The boundary conditions at the free surface, $z=\eta(x,y,t)$, are:

$$K_M(\frac{\partial u}{\partial z},\frac{\partial v}{\partial z})=(\tau_{0x},\tau_{0y})=C_d\rho_a(W_x W,\ W_y W) \quad \cdots\cdots(15)$$

$$\frac{\partial T}{\partial z}=\frac{\partial S}{\partial z}=0 \quad \cdots\cdots(16)$$

where C_d is drag coefficient; ρ_a is density of air; $\vec{W}=(W_x, W_y)$ is wind velocity. The value of drag coefficient C_d is given by(7)

$$C_d=(0.8+0.065W)\times10^{-3} \quad \cdots\cdots(17)$$

At bottom boundary,

$$u=v=w=0;\ \frac{\partial T}{\partial z}=\frac{\partial S}{\partial z}=0 \quad \cdots\cdots(18)$$

$$\rho_0 K_M\left(\frac{\partial u}{\partial z}, \frac{\partial v}{\partial z}\right)=(\tau_{bx}, \tau_{by}) = \rho_0 C_B |\vec{V_b}|\vec{V_b} \quad \cdots\cdots(19)$$

with value of the drag coefficient C_B given by

$$C_B=\left[\frac{1}{\kappa}\ln(H+z_b)/z_0\right]^{-2} \quad \cdots\cdots(20)$$

where z_0 is roughness height set to 0.2 cm in this study. At open boundary, tidal forcing is given by the fluctuation of free surface, i.e.,

$$\eta = A(M_2)\cos[\omega(M_2)t-g(M_2)] + A(S_2)\cos[\omega(S_2)t-g(S_2)] \quad \cdots\cdots(21)$$

where $A(M_2)$, $A(S_2)$, $\omega(M_2)$, $\omega(S_2)$, $g(M_2)$, $g(S_2)$ are amplitude, angular velocity, and phase of M_2 and S_2 respectively.

The model uses a σ coordinate in the vertical, i.e.,

$$\sigma=\frac{z-\eta}{H+\eta} \quad \cdots\cdots(22)$$

where η is the surface elevation and H is the depth below the mean tidal level. Thus, σ ranges from $\sigma=-1$ at $z=-H$ to $\sigma=0$ at $z=\eta$. The σ coordinate system can easily deal with significant topographical variability and can produce realistic bottom boundary layers which are important in shallow coastal waters.

4. Results and comparison with the observations

Equations (1)-(12) are discretized in finite difference forms and solved numerically. They are stepped forward in time using a leapfrog time scheme. The scheme is explicit in the advective transport terms, but the implicit treatment of the vertical diffusion terms is used to accomodate the small vertical spacing required to resolve the important top and bottom boundary layers without drastically reducing the time step as would be the case with the usual explicit scheme. The use of an implicit scheme results in a tri-diagonal matrix which is solved by a Gaussian elimination method(8). The stability condition imposed on the time step is the Courant condition of the form

$$\Delta t < \frac{1}{2}[c^2(1/\Delta x^2+1/\Delta y^2)]^{-1/2} \quad \cdots\cdots(23)$$

where Δx and Δy are grid sizes in the x and y directions and c is the phase speed of the free surface gravity wave. The model has $22\times45\times6$ grids in x, y and z directions respectively. Grid sizes of horizontal directions are $\Delta x=\Delta y=100m$, and in vertical direction, 6 layers have grid size of 1m, 2m, 3m, 3m, 3m, 3m from surface to bottom respectively. Time step Δt is set to 1.5 sec. which meets the stability condition.

The calculation was initialized with a zero velocity and surface elevation. Initial temperature and salinity field are set to constant value of 15 ℃ and 30 ‰ respectively. For the unit of 900MWe of Busan power plant, the mean value of the discharge is 130,000 m3l/hr; it induces velocities of 0.3 m/sec. For these conditions, the heated temperature elevation is 7℃. Simulation was conducted for no wind and wind blowing cases. For no wind conditions, only tidal effect of spring and neap tides was simulated. For wind blowing cases, south and north wind of

5m/sec with mean tidal condition was simulated. The model reached nearly equilibrium state after 2 tidal periods so that results were taken after 4 tidal periods.

Fig. 9 - 16 show the computational results of current fields. In spring tides, maximum surface current of about 20 cm/sec occurs at ebb tide because directions of surface warm water discharges from the outfall of power plant coincides with that of ebb current(Fig. 9a). But flood current becomes considerably weak as the opposite direction of warm water discharges and flood current(Fig. 10a). At the convergence area, the eddy-like features are found which confirms field data of both Lagrangian and Eulerian measurements. Near bottom current(4th layer) shows contrary velocity distribution to the surface i.e., weak current in ebb and strong current in flood(Fig. 9b, 10b). This seems to be the compensational effect of surface and near bottom current. Warm water discharges are deflected toward the west side coast which seems to be the influence of the Coriolis effect. In north wind bolowing cases, strong current developes in ebb tides because of same directions of warm water discharges, ebb currents, and winds(Fig. 13a). Current flows southward along the both sides coasts without deflection to the east coast. But in flood tides, current flows northward along the central part of the bay while southward flow also found along the west side coast which is the wind-driven current (Fig. 14a). This causes counter-clockwise eddy-like features in the flow field. Compensational effect also occurs on surface and bottom current. In ebb tides, near bottom current flows weakly southward, but in flood tides, northward flow developes somewhat strongly along the central part of the bay. South wind blowing case is contrary to the north wind blowing case. In flood tides, with the help of the wind, flood current flows stongly northward and developes more along the west side coast(Fig. 16a). In ebb tides, southward flow developes along the central part of the bay while northward flow exists along the west side which results in clockwise eddy-like features(Fig. 15a). Near bottom current flows southward shifted to the east coast in ebb tides(Fig. 15b). No flows develope along the west side coast while in flood tides, it flows along the west side coast(Fig. 16b).

In Fig. 17 - 18, excess temperature distributions at spring and neap tides are represented. Isotherms are generally runs northeast-southwest directions which in turn suggests the deflection of the warm water discharges to the west side coast. Observational results nearly coincides with computational results such as tongue-like features near the outfall and higher teperature on the west side coast(Fig. 3 and Fig. 18a). But in Fig. 2, the observational distributions are somewhat diffrent to the computational results on the point that isotherms run northwest-southeast direction. This can be explained as the advection effect of both wind and the flood current flowing mainly along the west side coast.

5. Conclusion

Three dimensional $k-\varepsilon$ turbulence closure model is used to simulate the circulation characteristics in the nearly closed bay and applied to Gamcheon bay in Pusan, Korea comparing with the observations. Some eddy-like features are found to exist in Gamcheon bay from the observations and computational results. Compensational flows exist between surface and bottom current. Model

simulations well agree with the observations. Further study is required to analyse the complicated circulation and to investigate the eddy-like structures thoroughly.

Acknowledgements

The authors wish to acknowledge the financial support of the Korea Research Founddation made in the Program Year 1996.

요 약

한국의 부산에 위치한 감천만에서의 해수유동을 파악하기 위하여 3차원 유동모델을 사용하여 계산을 하고 그 결과를 관측치와 비교하였다. 모델은 개방경계에서의 조석, 바람, 화력발전소에서의 온배수에 의해 힘을 받아 해수유동을 재현한다. 난류혼합계수는 $k-\varepsilon$난류클로즈 모델의 의해 계산하였다. 수온, 염분, 해조류를 현장관측하여 관측자료와 모델결과를 비교하였다. 소용돌이 형태의 흐름이 현장관측자료와 모델결과에서 관측되었는데 이는 약한 조류와, 풍성류, 온배수의 상호작용에 의해 형성된 것으로 분석되어진다. 표층과 저층의 흐름은 서로 연관되어 있는데 즉, 표층의 흐름이 강해지면 저층의 흐름이 약해지고 반대의 경우도 성립한다.

References

1) Leenderts, J. J. and Liu, S. K., A three dimensional model for estuaries and coastal seas, Aspects of computaion, Rep. R-1764-OWRT, Rand Inst. Santa Monica, Calif., Vol. 2, (1973).
2) Heaps, N. S., A three dimensional numerical model of the Irish Sea, Geophys. J. Astron. Soc., Vol. 35, (1973), p.99.
3) Sundermann, J., A three dimensional model of a homogeneous estuary, in Proceedings of the Fourteenth Coastal Engineering Conference, Copenhagen, 1974, American Society of Civil engineering, Vol. 3, (1975), p.2337
4) Eckart, C., Properties of water; Part II: The equation of state of water and sea water at low temperatures and pressures, American J. of Science, Vol. 256, (1958), p.225.
5) McGuirk, J. J. and Rodi, W., Mathematical modelling of three - dimensional heated surface jets, J. Fluid Mech., Vol. 95, No. 4(1979), p.609.
6) Rodi, W., Turbulence models and their application in hydraulic - a state of the art review, Institute fur Hydromechanik, University of Karlsruhe, 1984.
7) Wu, J., Wind stress coefficients over sea surface near neutral condition, J. Phys. Oceanogr., Vol. 10, No. 5(1980), p.727.
8) Richtmyer, R. D., and Morton, K. W., Difference methods for initial-value problems, 2nd. ed., Interscience, New York, 1967.

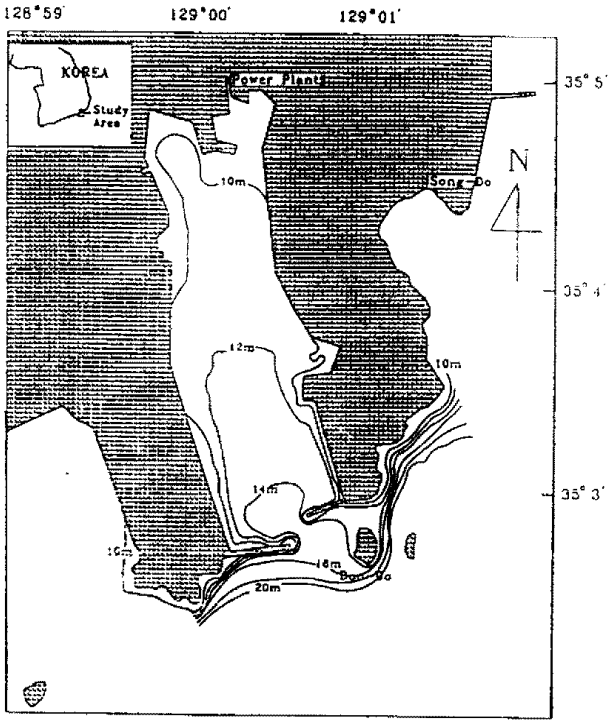

Fig. 1 Location and bathymetry of study area

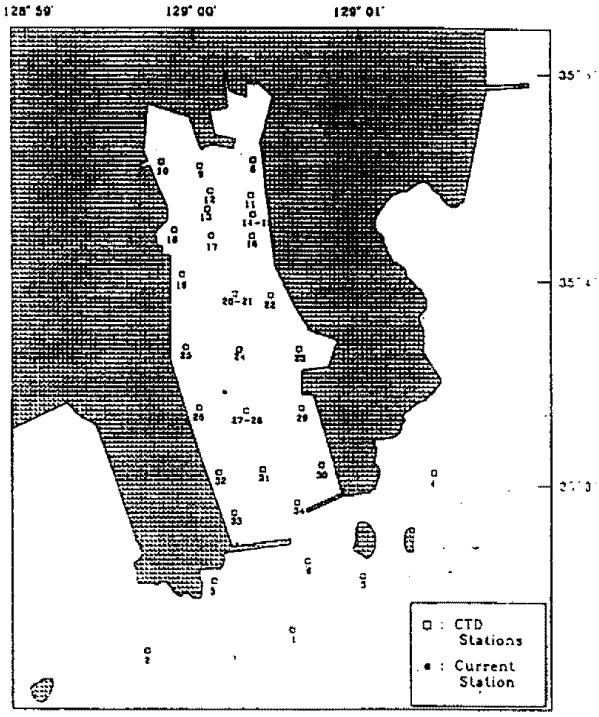

Fig. 2 Stations of CTD and current measurements

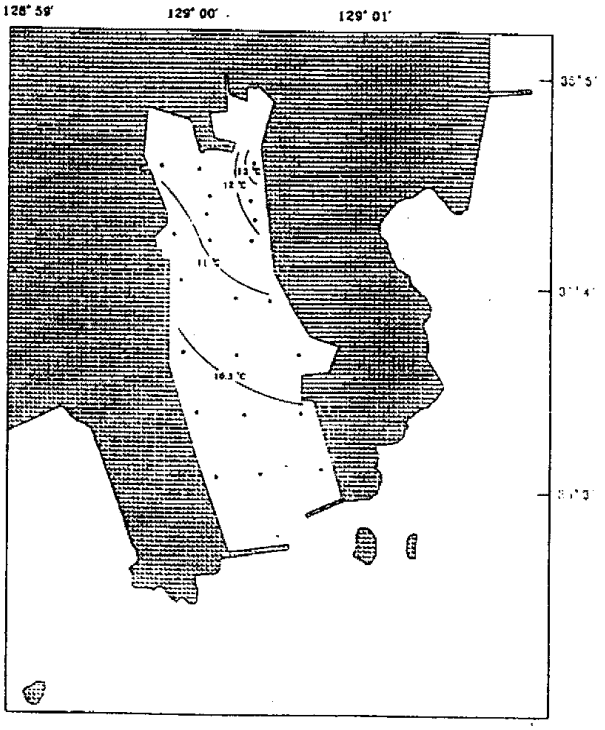

Fig. 3 Surface temperature distribution on February 26, 1996

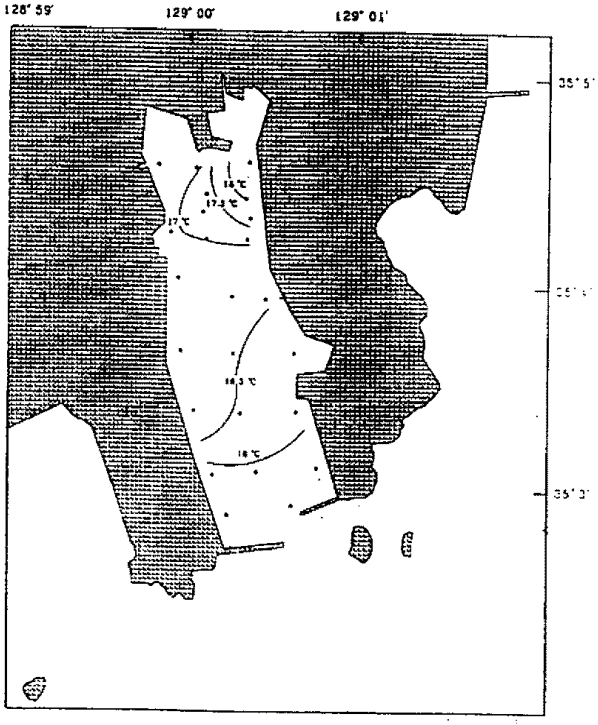

Fig. 4 Surface temperature distribution on May 17, 1996

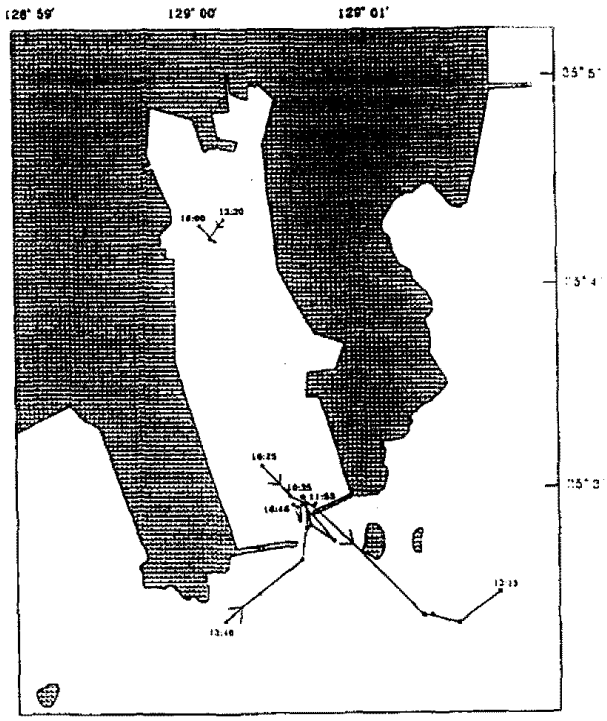

Fig. 5 Lagrangian tracking of surface flow by drogue on February 28, 1996

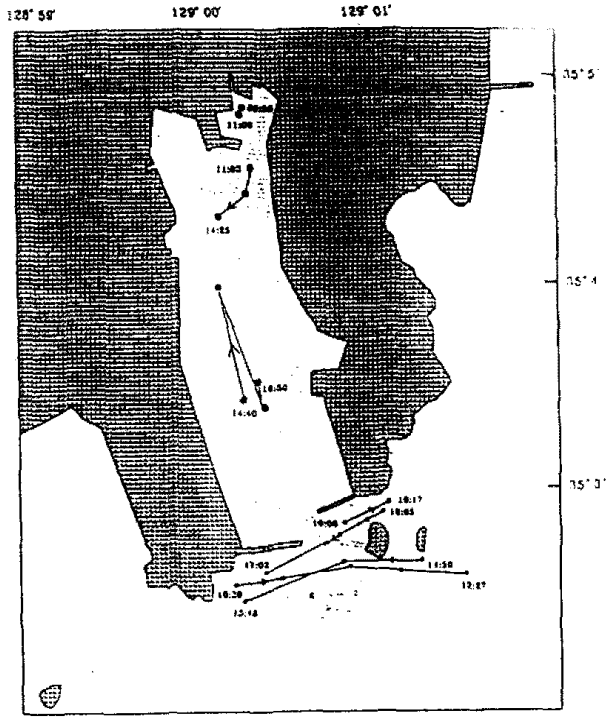

Fig. 6 Lagrangian tracking of surface flow by drogue on May 18, 1996

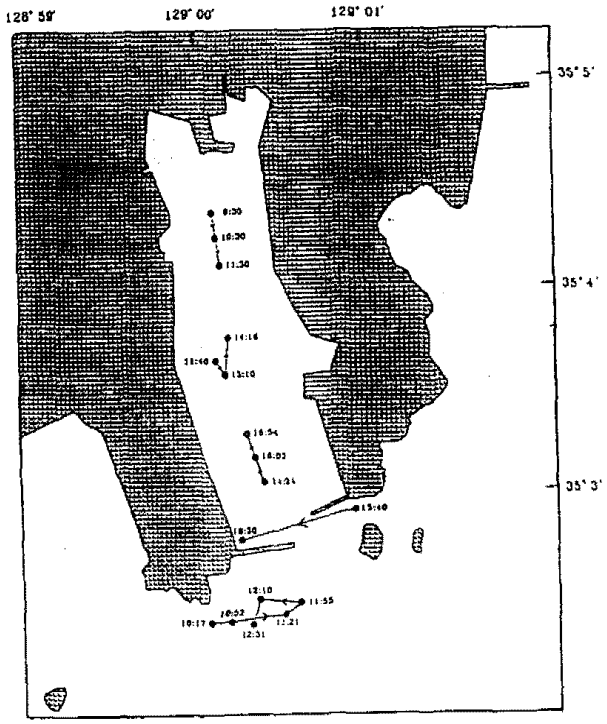

Fig. 7 Lagrangian tracking of surface flow by drogue on July 26, 1996

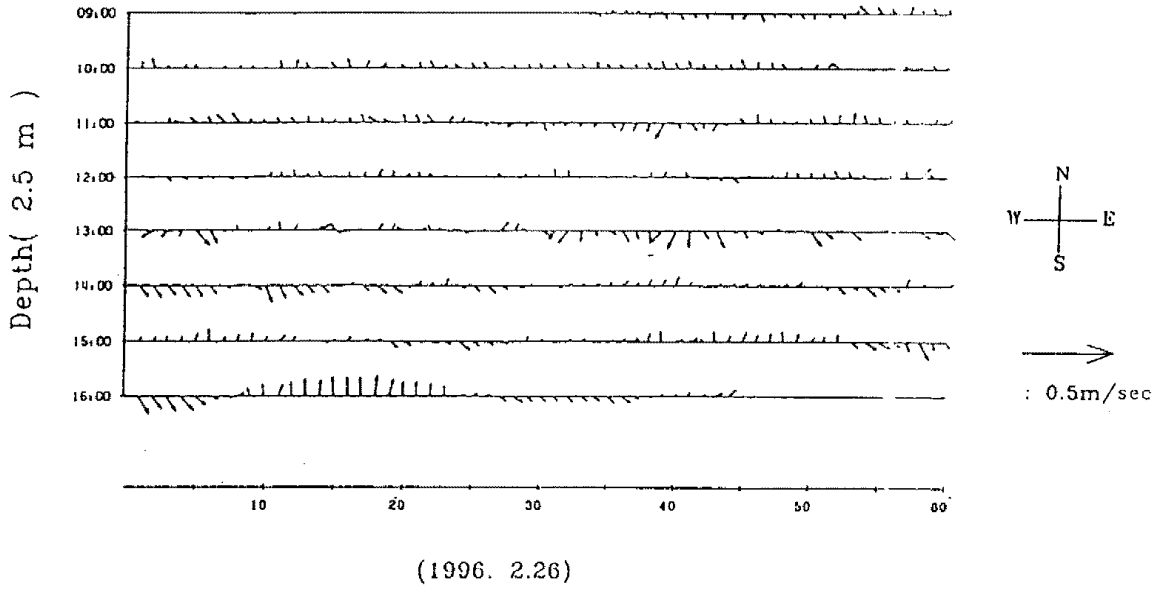

Fig. 8a Time series of Eulerian measurements of surface current on February 28, 1996

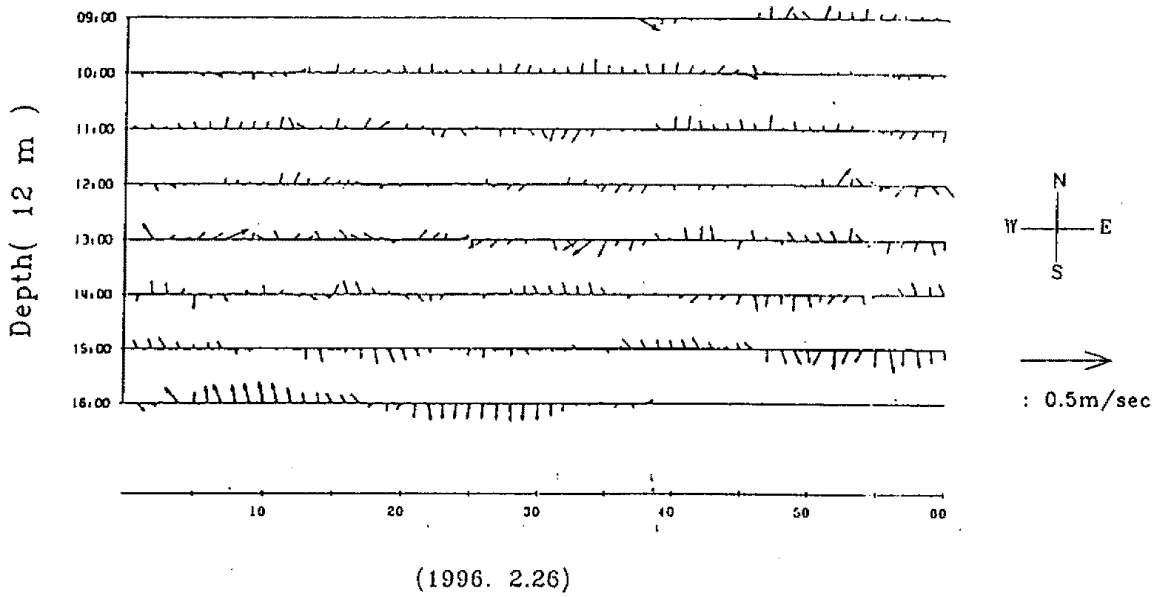

Fig. 8b Time series of Eulerian measurements of bottom current on February 28, 1996

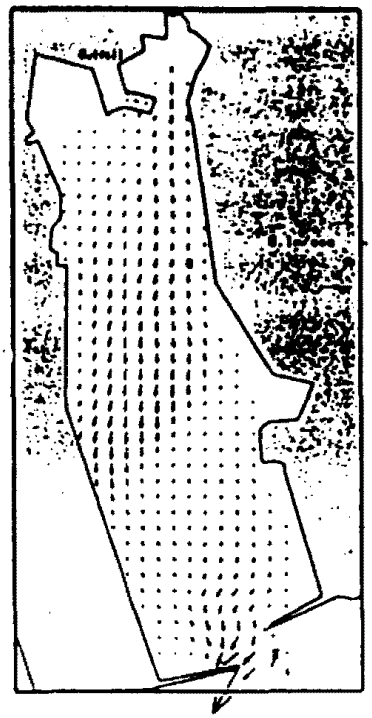

Fig. 9a Maximum ebb current field of surface layer with no winds in spring tides

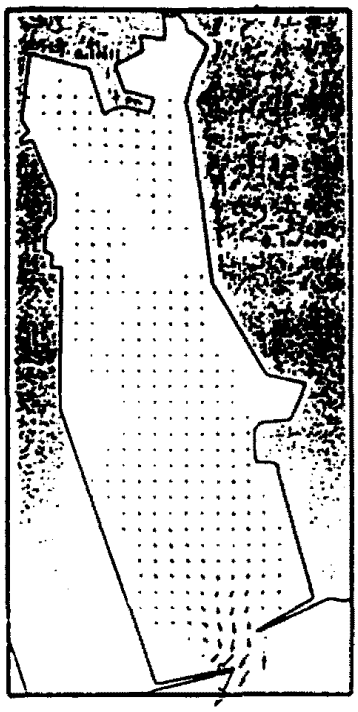

Fig. 9b Maximum ebb current field of fourth layer with no winds in spring tides

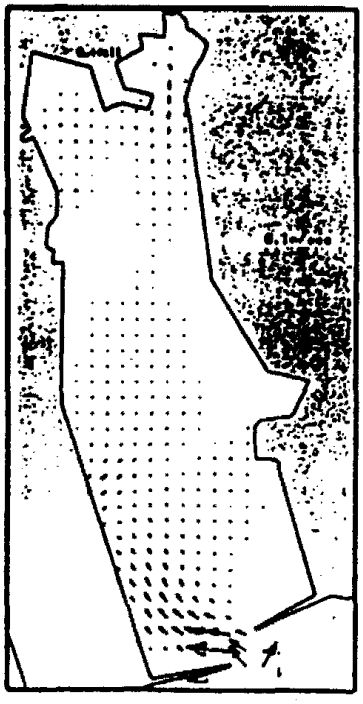

Fig. 10a Maximum flood current field of surface with no winds in spring tides

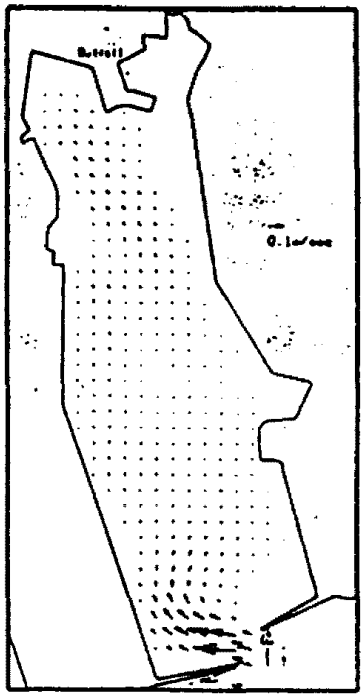

Fig. 10b Maximum flood current field of fourth layer with no winds in spring tides

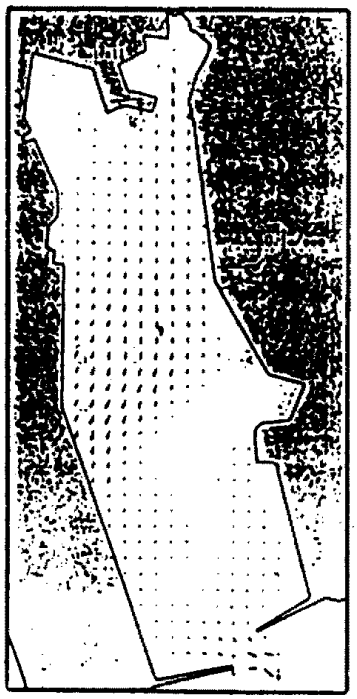

Fig. 11a Maximum ebb current field of surface layer with no winds in neap tides

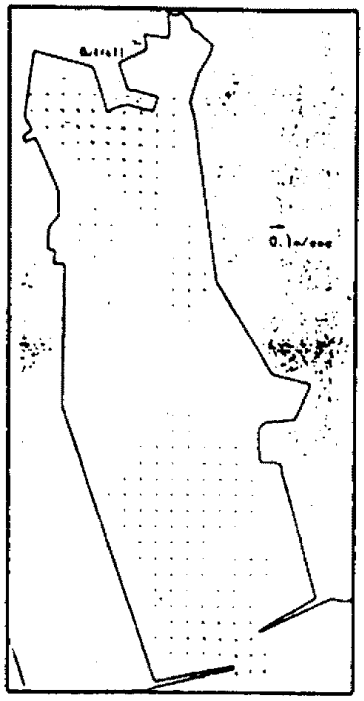

Fig. 11b Maximum ebb current field of fourth layer with no winds in neap tides

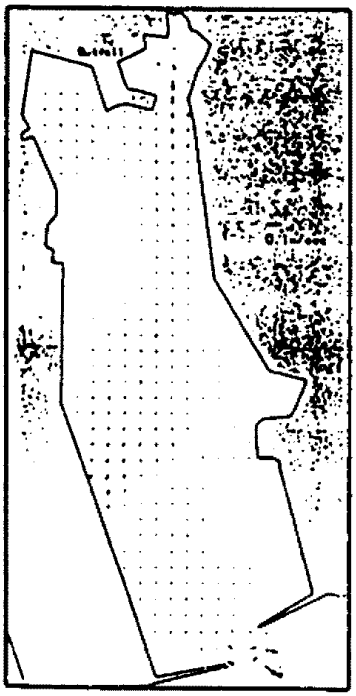

Fig. 12a Maximum flood current field of surface layer with no winds in neap tides

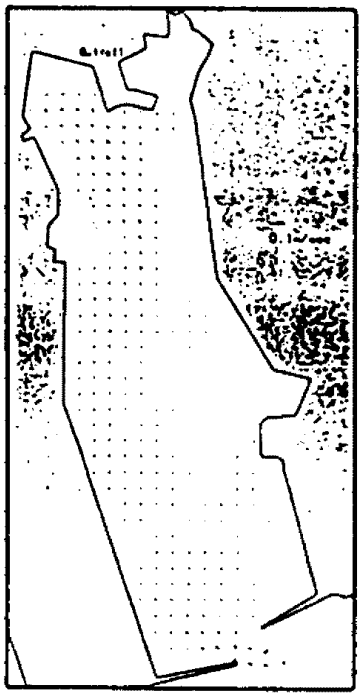

Fig. 12b Maximum flood current field of fourth layer with no winds in neap tides.

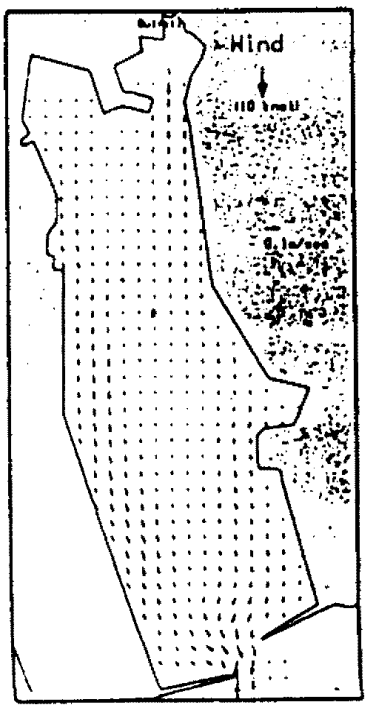

Fig. 13a Maximum ebb current field of surface layer with north winds

Fig. 13b Maximum ebb current field of fourth layer with north winds.

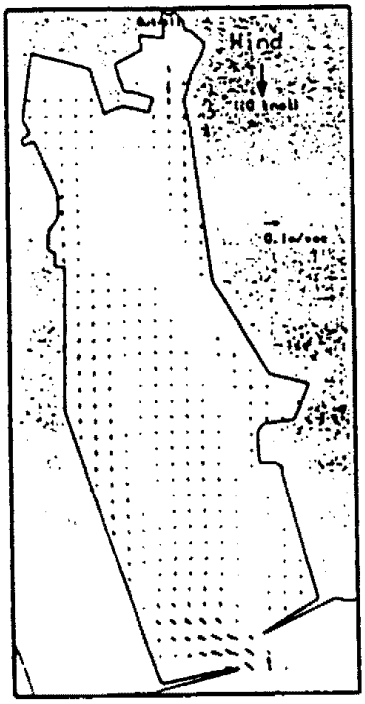

Fig. 14a Maximum flood current field of fourth surface layer with north winds.

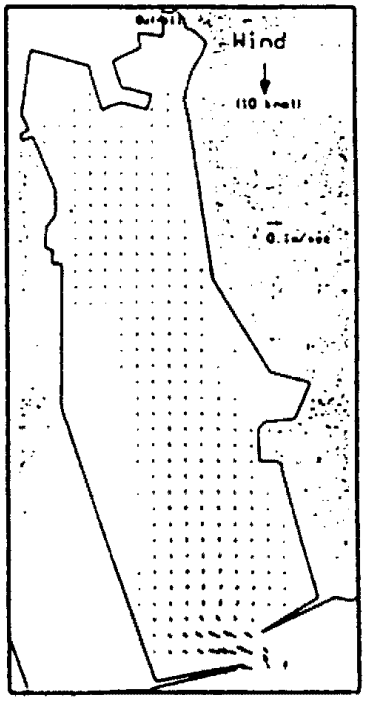

Fig. 14b Maximum flood current field of fourth layer with north winds.

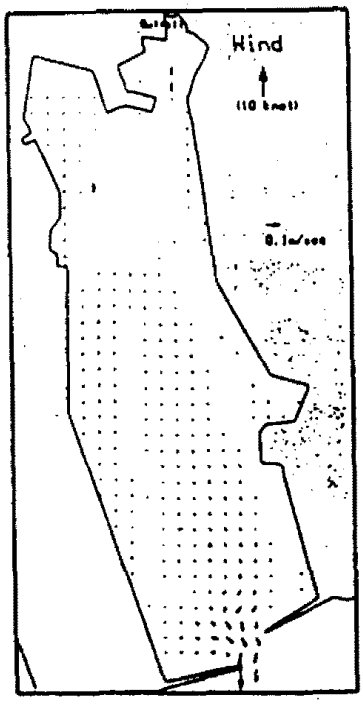

Fig. 15a Maximum ebb current field of surface layer with south winds.

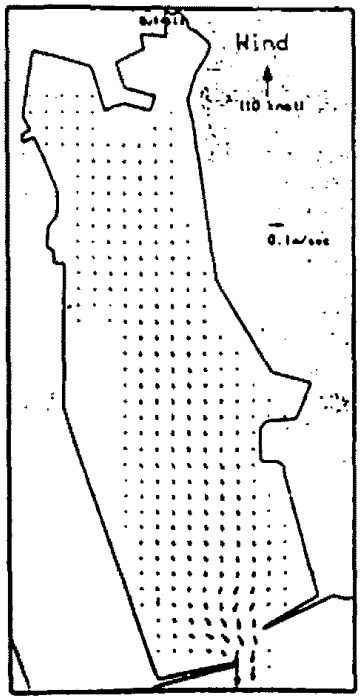

Fig. 15b Maximum ebb current field of fourth layer with south winds.

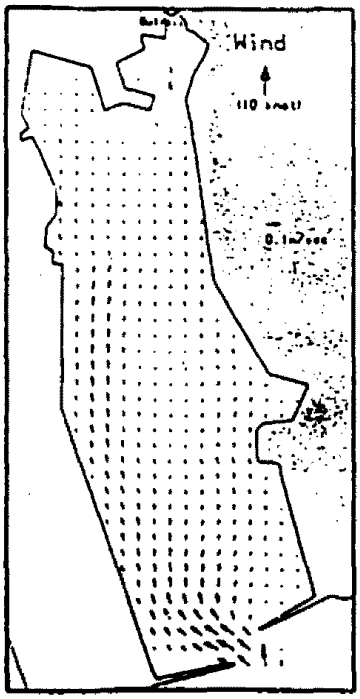

Fig. 16a Maximum flood current field of fourth layer with south winds.

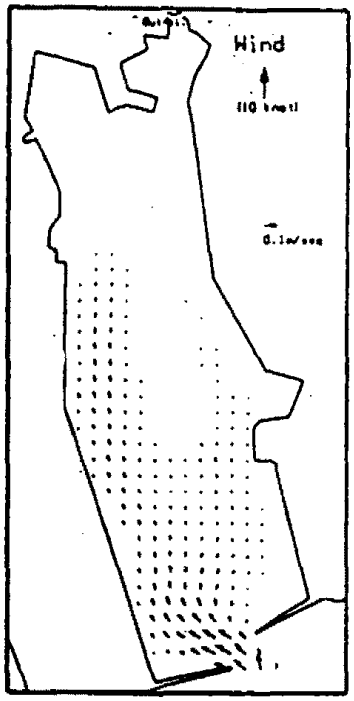

Fig. 16b Maximum flood current field of fourth layer with south winds

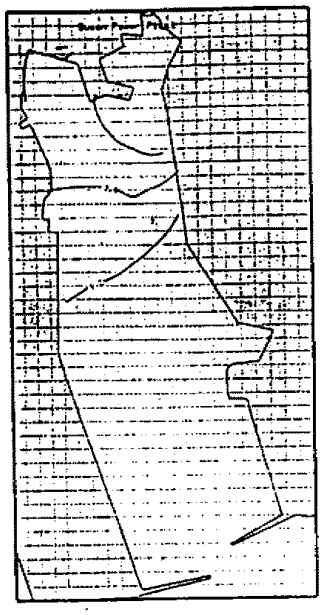

Fig. 17a Excess temperature distributions of surface layer at maximum flood current in spring tides.

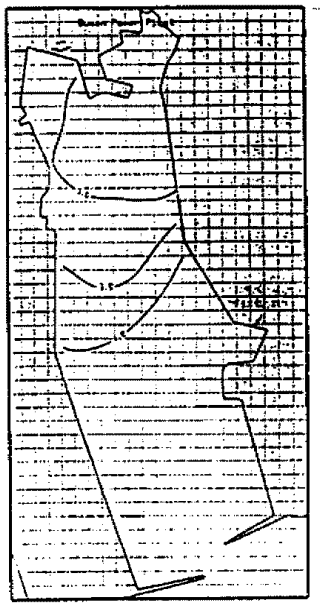

Fig. 17b Excess temperature distributions of surface layer at maximum ebb current in spring tides.

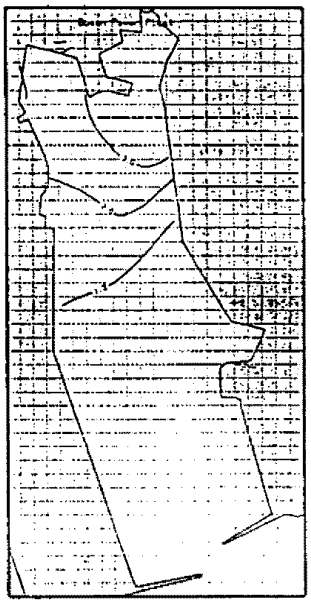

Fig. 18a Excess temperature distributions of surface layer at maximum flood current in neap tides.

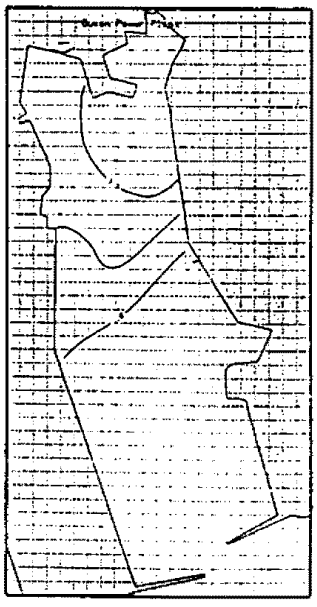

Fig. 18b Excess temperature distributions of surface layer at maximum ebb current in neap tides.